

ganisms to landscape structure (6), generalizations for the design and management of agricultural landscapes are still a matter for future research.

References and Notes

1. P. Kareiva, *Philos. Trans. R. Soc. London* **330**, 175 (1990); A. Kruess and T. Tschamtkke, *Science* **264**, 1581 (1994); T. Tschamtkke and A. Kruess, in *Theoretical Approaches to Biological Control*, B. A. Hawkins and H. V. Cornell, Eds. (Cambridge Univ. Press, Cambridge, 1999), pp. 190–205.
2. P. Jourdeuil, *Ann. Epiphyt.* **11**, 445 (1960).
3. H. Hokkanen, G. Husberg, M. Söderblom, *Ann. Agric. Fenn.* **27**, 281 (1988).
4. W. Powell, in *Insect Parasitoids*, J. Waage and W. Greathead, Eds. (Academic Press, London, 1986), pp. 319–340; R. C. van Driesche and T. S. Bellows, *Biological Control* (Chapman & Hall, New York, 1996).
5. L. Hansson, L. Fahrig, G. Merriam, Eds., *Mosaic Landscapes and Ecological Processes* (Chapman & Hall, London, 1995); P. C. Marino and D. A. Landis, *Ecol. Appl.* **6**, 276 (1996); F. D. Menalled, P. C. Marino, S. H. Gage, D. A. Landis, *ibid.* **9**, 634 (1999).
6. J. Roland and P. D. Taylor, *Nature* **386**, 710 (1996).
7. Field margin strips were 3 m wide, about 100 m long, and either 1 year old or 6 years old. The 1-year-old field margin strips included naturally developed vegetation ($N = 4$), sown *Phacelia tanacetifolia* strips ($N = 4$), sown wildflower mixtures of 19 species ($N = 4$), and sown (monoculture) wheat ($N = 4$). The six-year-old field margin strips ($N = 4$) were naturally developed. Each of four studied rape fields was surrounded by all five types of field margins in the same structurally simple landscape.
8. Experimental summer rape plots (2 m² of sown rape plots; $N = 12$) were placed in three types of habitats: (i) large fallows (>1 ha, 6 years old with naturally developed vegetation) and (ii) small (3-m-wide) field margin strips (6 years old with naturally developed vegetation), and (iii) monocultural rape fields as the control (Fig. 1B). In addition, we also examined the effects of these habitat types on winter rape crop fields ($N = 16$) (Fig. 1C).
9. Landscape structure was estimated in 15 circular landscape profiles with a diameter of 1.5 km by using aerial photographs and intensive field inspections. The area of each habitat type was measured. Non-crop area includes all uncultivated and perennial habitats such as fallows, field margins, grassland, hedges, and woods. The diversity of habitat types was calculated following Shannon's index. The isolation of a sampling site i from surrounding noncrop area (indexed by j) was measured indirectly by a negative exponential weighting function, $Isolation_i = -\sum (e^{-Distance} \times non-crop\ area_j) / \sum e^{-Distance}$ [see, for example, S. Eber, R. Brandl, *J. Anim. Ecol.* **65**, 621 (1996)].
10. Parasitism was studied during the full-flowering period of rape in May (unsprayed winter rape fields) and June (experimental summer rape plots). All summer rape flowers of five randomly selected plants were collected in each of the 12 experimental plots in different habitats (Fig. 1B) and in each of the 15 experimental plots in different landscapes (Fig. 2B). In each landscape, plots out of two pots (volume, 30 liters; five plants per pot) were established in old field margin strips adjacent to cereal fields. Winter rape flowers were sampled near the edge (1 m into the field) and toward the center of the fields (10 to 12 m into the field): (i) 20 independent samples (each sample with two subsamples of 40 flowering shoots) in winter rape fields adjacent to five different types of field margin strips with four replicates each (Fig. 1A); (ii) 16 independent samples (each with two subsamples comprising all flowers from 0.25 m²) in winter rape fields adjacent to three different habitat types with five to six replicates each (Fig. 1C); and (iii) 15 independent samples (each with two to four subsamples comprising all flowers from 0.25m²) in the 15 landscapes (Fig. 2D). Rates of parasitism were measured by dissection of last instar larvae of rape pollen beetle. Plant damage caused by feeding of

adult pollen beetles was assessed by the number of destroyed buds, which did not develop into pods and appeared as podless stalks (Fig. 2, A and C).

11. C. Nilsson, *Z. Angew. Entomol.* **100**, 302 (1985).
12. C. Börner and H. Blunk, *Mitt. Biol. Reichsanst. Land Forstwirtschaft. Berlin* **18**, 91 (1920).
13. Our experiments also showed that pollen and nectar resources as well as alternative hosts had no significant effect on parasitoid enhancement, although flower availability greatly differed between field margin types, from the sowings with wheat (as a control) to sowings with species-rich wildflower mixtures.
14. Rates of parasitism (Y) were correlated with the percentage of noncrop area (X) in both parasitoid species. *Tersilochus heteroceris*: $Y = 4.5 + 0.46X$, $F = 5.18$, $P = 0.04$, coefficient of determination $R^2 = 0.285$, $N = 15$ (field edge); and $Y = 6.7 + 0.54X$, $F = 10.2$, $P = 0.008$, $R^2 = 0.44$, $N = 15$ (field center). *Phradis interstitialis*: mean rate = 32.7%, $P =$ not significant (field edge); and $Y = 1/(0.02 + 0.38/X)$, $F = 10.01$, $P = 0.007$, $R^2 = 0.44$, $N = 15$ (field center). High rates of parasitism in complex landscapes were also related to

high rates of multiparasitism (Y). Attack of one host larvae by the two parasitoid species at the same time did significantly increase with noncrop area (X), on average from 2 to 27% ($Y = 4.5 + 0.46X$, $F = 15.4$, $P = 0.002$, $R^2 = 0.54$, $N = 15$) at the edge, and from 2 to 32% ($Y = 2.4 + 0.4X$, $F = 32.3$, $P < 0.001$, $R^2 = 0.73$, $N = 15$) in the center of the fields.

15. Pflanzenschutzamt Hannover, *Empfehlungen Pflanzenschutz 1998/1999* (Diaprint, Hanover, Germany, 1998).
16. B. A. Hawkins and H. V. Cornell, *Science* **266**, 1886 (1994).
17. We thank R. Dolch, B. Ekbohm, A. Kruess, D. A. Landis, M. Steinwachs-McClure, and two anonymous reviewers for comments on the manuscript, and J. Kuhnhenne for technical assistance. Supported by the German Ministry of Environment (Bundesministerium für Umwelt und Reaktorsicherheit), the German Science Foundation (Deutsche Forschungsgemeinschaft), and the Forschungs- und Studienzentrum Landwirtschaft und Umwelt, Göttingen.

23 March 1999; accepted 7 July 1999

Signaling from Rho to the Actin Cytoskeleton Through Protein Kinases ROCK and LIM-kinase

Midori Maekawa,¹ Toshimasa Ishizaki,¹ Shuken Boku,¹ Naoki Watanabe,¹ Akiko Fujita,¹ Akihiro Iwamatsu,² Takashi Obinata,³ Kazumasa Ohashi,⁴ Kensaku Mizuno,⁴ Shuh Narumiya^{1*}

The actin cytoskeleton undergoes extensive remodeling during cell morphogenesis and motility. The small guanosine triphosphatase Rho regulates such remodeling, but the underlying mechanisms of this regulation remain unclear. Cofilin exhibits actin-depolymerizing activity that is inhibited as a result of its phosphorylation by LIM-kinase. Cofilin was phosphorylated in N1E-115 neuroblastoma cells during lysophosphatidic acid-induced, Rho-mediated neurite retraction. This phosphorylation was sensitive to Y-27632, a specific inhibitor of the Rho-associated kinase ROCK. ROCK, which is a downstream effector of Rho, did not phosphorylate cofilin directly but phosphorylated LIM-kinase, which in turn was activated to phosphorylate cofilin. Overexpression of LIM-kinase in HeLa cells induced the formation of actin stress fibers in a Y-27632-sensitive manner. These results indicate that phosphorylation of LIM-kinase by ROCK and consequently increased phosphorylation of cofilin by LIM-kinase contribute to Rho-induced reorganization of the actin cytoskeleton.

During cell morphogenesis and motility, cells undergo extensive remodeling of the actin cytoskeleton, a phenomenon that is mediated by various actin-binding proteins (1). Such remodeling is often triggered by extracellular stimuli, but the signaling pathways to actin-binding proteins remain largely uncharacterized. The small guanosine triphosphatase

(GTPase) Rho is converted from the inactive, guanosine diphosphate-bound form to the active, GTP-bound form in response to stimuli such as serum and lysophosphatidic acid (LPA), and induces various morphological events such as cell adhesion and motility (2). Among Rho effectors isolated, the ROCK family of Rho-associated serine-threonine protein kinases is implicated in Rho-mediated cell adhesion and smooth muscle contraction (2). These kinases phosphorylate myosin light chain (MLC) phosphatase and inhibit its activity (3); this inhibition, in turn, results in an increase in MLC phosphorylation and, consequently, increases actomyosin-based contractility, events that contribute to Rho-mediated stress fiber formation and smooth mus-

¹Department of Pharmacology, Kyoto University Faculty of Medicine, Kyoto 606-8315, Japan. ²Central Laboratories for Key Technology, Kirin Brewery, Yokohama 236-0004, Japan. ³Department of Biology, Faculty of Science, Chiba University, Chiba 263-8522, Japan. ⁴Biological Institute, Graduate School of Science, Tohoku University, Sendai 980-8578, Japan.

*To whom correspondence should be addressed. E-mail: snaru@mfour.med.kyoto-u.ac.jp

REPORTS

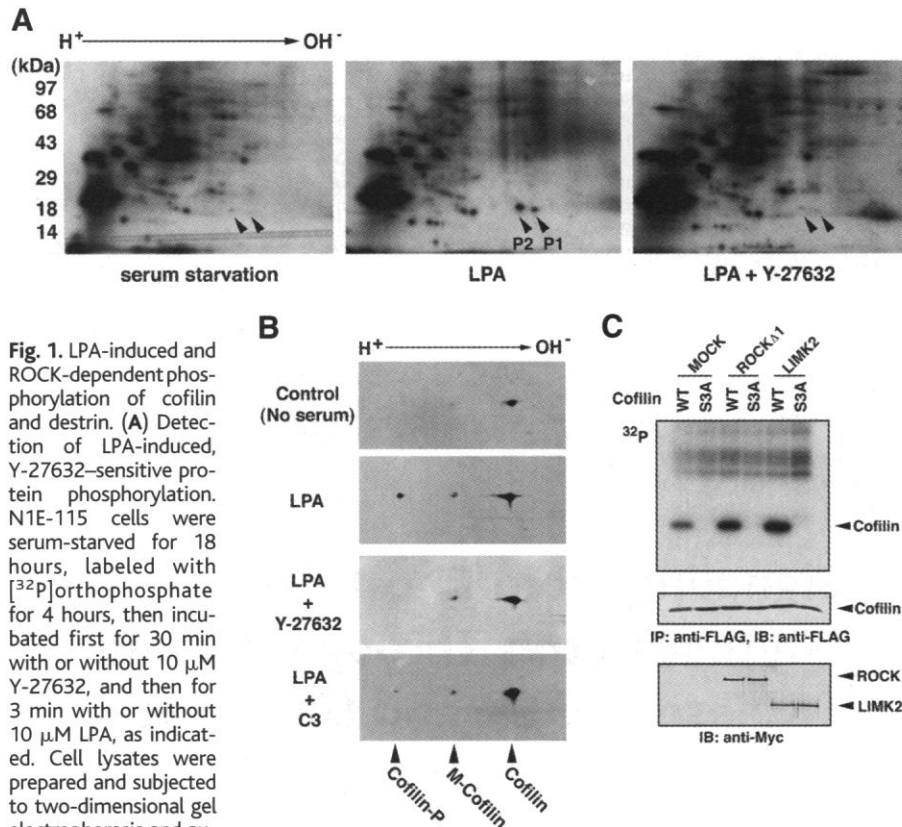


Fig. 1. LPA-induced and ROCK-dependent phosphorylation of cofilin and destrin. (A) Detection of LPA-induced, Y-27632-sensitive protein phosphorylation. N1E-115 cells were serum-starved for 18 hours, labeled with [³²P]orthophosphate for 4 hours, then incubated first for 30 min with or without 10 μM Y-27632, and then for 3 min with or without 10 μM LPA, as indicated. Cell lysates were prepared and subjected to two-dimensional gel electrophoresis and autoradiography. Two proteins (P1 and P2) whose phosphorylation was induced by LPA and inhibited by Y-27632 are indicated. (B) Immunoblot analysis of cofilin phosphorylation. N1E-115 cells were serum-starved with or without C3 exoenzyme (30 μg/ml), and then treated with Y-27632 and LPA as described above. Cell lysates were prepared and subjected to two-dimensional gel electrophoresis and immunoblot analysis with MAB22 antibody specific for cofilin. The labels cofilin, M-cofilin, and cofilin-P indicate unphosphorylated forms of nonmuscle-type and muscle-type cofilin and a phosphorylated form of nonmuscle-type cofilin, respectively. (C) ROCK-dependent cofilin phosphorylation. COS-7 cells expressing FLAG-tagged wild-type (WT) cofilin or its S3A mutant either alone (mock) or with Myc-tagged ROCKΔ1 or Myc-tagged LIM-kinase 2 (LIMK2) were labeled with [³²P]orthophosphate and then lysed. Cell lysates were subjected to immunoprecipitation (IP) with antibodies to FLAG. The precipitates were analyzed by SDS-PAGE and autoradiography (top) or by immunoblot (IB) with antibodies to FLAG (middle). Cell lysates were probed with antibodies to Myc (bottom). The positions of cofilin, ROCKΔ1, and LIMK2 are indicated.

cle contraction (4, 5). Although these kinases phosphorylate other actin-related proteins in vitro (6), whether such phosphorylation also occurs in vivo remains unknown.

In serum-free medium, N1E-115 neuroblastoma cells become flattened and extend neurites. Addition of LPA to these cells causes neurite retraction, which is mediated by Rho and completes within 5 min (7). This neurite retraction is accompanied by an increase in MLC phosphorylation, and both are prevented by exposure of the cells to Y-27632, a specific inhibitor of ROCK (8). We therefore investigated whether other ROCK substrates also contribute to this process. We used two-dimensional gel electrophoresis and autoradiography to detect ROCK targets whose phosphorylation is induced by LPA and inhibited by Y-27632 (Fig. 1A) (9). The phosphorylation of two proteins with apparent molecular sizes of 19 kD (P1) and 20 kD (P2) increased in cells treated with

LPA. The LPA-induced phosphorylation of these proteins was inhibited by treatment of cells with Y-27632. As seen in other ROCK-mediated processes (5, 8), this phosphorylation was almost completely inhibited at 10 μM Y-27632, suggesting that it occurs as a consequence of Rho-ROCK signaling. P1 and P2 proteins were isolated and subjected to proteolytic digestion and mass spectrometry (10). On the basis of peptide fingerprints, P1 and P2 were identified as destrin and nonmuscle-type cofilin, respectively. Both destrin and cofilin belong to the actin-depolymerizing factor/cofilin family with filamentous (F)-actin-severing and F-actin-depolymerizing activities (11).

We used immunoblot analysis with a monoclonal antibody to cofilin (12) to examine whether endogenous cofilin was phosphorylated on exposure of N1E-115 cells to LPA. LPA induced phosphorylation of cofilin in a Y-27632-sensitive manner (Fig. 1B). C3 exo-

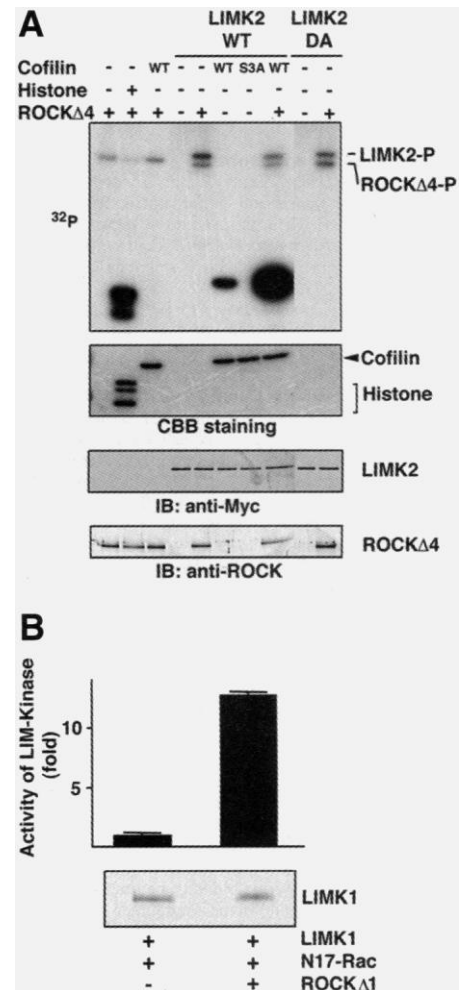


Fig. 2. Mediation of ROCK-induced phosphorylation of cofilin by LIM-kinase. (A) Phosphorylation and activation of LIM-kinase by ROCK in vitro. Myc-tagged WT LIMK2 or its D451A mutant (DA) prepared from COS-7 cells was subjected to in vitro kinase reactions with [³²P]ATP with or without cofilin (WT or S3A) as substrate, and in the absence or presence of ROCKΔ4. The kinase activity of ROCKΔ4 was also assayed with histone as substrate. Protein phosphorylation was analyzed by SDS-PAGE and autoradiography (top). Gels were also stained with Coomassie brilliant blue (CBB) (upper middle) and subjected to immunoblot analysis with antibodies to Myc (lower middle) or to ROCK (bottom). The positions of the various proteins are indicated, with LIMK2-P and ROCKΔ4-P referring to phosphorylated LIMK2 and ROCKΔ4, respectively. ROCKΔ4 was also shown to activate LIMK1 in vitro (18). (B) Activation of LIM-kinase by ROCK in vivo. FLAG-tagged LIMK1 and FLAG-tagged N17-Rac were expressed in COS-7 cells either alone or together with Myc-tagged ROCKΔ1. LIMK1 was immunoprecipitated with antibodies to FLAG and subjected to in vitro kinase reactions with cofilin as substrate. Phosphorylation was quantified by an image analyzer. The kinase activity is expressed as the mean ± SEM (n = 3) relative to the value for cells not expressing ROCKΔ1 (top). In vivo activation of LIMK2 by ROCKΔ1 was also observed (18).

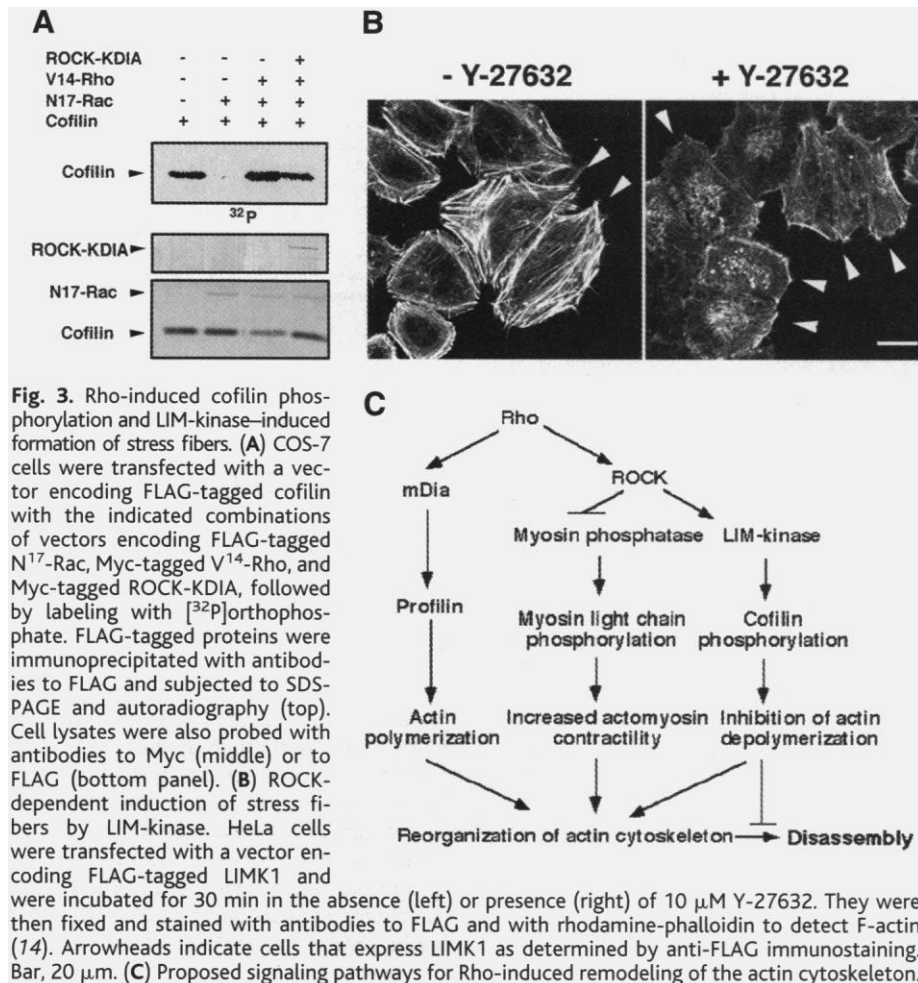


Fig. 3. Rho-induced cofilin phosphorylation and LIM-kinase-induced formation of stress fibers. **(A)** COS-7 cells were transfected with a vector encoding FLAG-tagged cofilin with the indicated combinations of vectors encoding FLAG-tagged N¹⁷-Rac, Myc-tagged V¹⁴-Rho, and Myc-tagged ROCK-KDIA, followed by labeling with [³²P]orthophosphate. FLAG-tagged proteins were immunoprecipitated with antibodies to FLAG and subjected to SDS-PAGE and autoradiography (top). Cell lysates were also probed with antibodies to Myc (middle) or to FLAG (bottom panel). **(B)** ROCK-dependent induction of stress fibers by LIM-kinase. HeLa cells were transfected with a vector encoding FLAG-tagged LIMK1 and were incubated for 30 min in the absence (left) or presence (right) of 10 μ M Y-27632. They were then fixed and stained with antibodies to FLAG and with rhodamine-phalloidin to detect F-actin (14). Arrowheads indicate cells that express LIMK1 as determined by anti-FLAG immunostaining. Bar, 20 μ m. **(C)** Proposed signaling pathways for Rho-induced remodeling of the actin cytoskeleton.

enzyme, which inactivates Rho by ADP ribosylation (2), also inhibited LPA-induced phosphorylation of cofilin. We confirmed that the P2 spot overlapped exactly with the spot at which phosphorylated cofilin migrated during gel electrophoresis. These results corroborated the data obtained by ³²P labeling and demonstrated a net increase in the amount of phosphorylated cofilin during neurite retraction.

We then investigated whether active ROCK induced phosphorylation of cofilin in vivo (13). Expression of ROCK Δ 1, a dominant active ROCK mutant (14), with cofilin in COS-7 cells resulted in an increase in the extent of ³²P incorporation into cofilin (Fig. 1C). Cofilin is phosphorylated or dephosphorylated at Ser³ under various physiological conditions, with the phosphorylated form of the protein being inactive (11, 15). A cofilin mutant (S3A) in which this serine residue is replaced by alanine was not phosphorylated in cells expressing ROCK Δ 1, suggesting that ROCK induces cofilin phosphorylation at the physiological phosphorylation site.

To determine whether cofilin is a direct substrate of ROCK, we incubated cofilin with active ROCK in vitro (16). ROCK did not directly phosphorylate cofilin (Fig. 2A), in-

dicating that the effect of ROCK in intact cells is mediated through the action of another kinase. LIM-kinase phosphorylates cofilin at Ser³ both in vitro and in vivo (17). We therefore investigated whether LIM-kinase functions as an intermediary between ROCK and cofilin. LIM-kinase 2 (LIMK2) prepared from COS-7 cells was incubated with cofilin in the absence or presence of active ROCK. Consistent with previous results (17), LIMK2 phosphorylated wild-type cofilin but not its S3A mutant. Intriguingly, cofilin phosphorylation by LIMK2 was greatly enhanced in the presence of ROCK (Fig. 2A). LIMK2 was also phosphorylated in the presence of active ROCK, as was a kinase-defective LIMK2 mutant (LIMK2-DA). These results indicate that ROCK phosphorylates LIM-kinase and thereby increases its kinase activity toward cofilin. We also examined whether ROCK induces activation of LIM-kinase in vivo. LIMK1 was expressed in COS-7 cells in the absence or presence of ROCK Δ 1, and was immunoprecipitated (13). The kinase activity of LIMK1 immunoprecipitated from cells co-expressing ROCK Δ 1 was ~13 times that of the enzyme recovered from cells not expressing ROCK Δ 1 (Fig. 2B).

Our data indicate that cofilin phosphorylation by LIM-kinase occurs as a consequence of activation of Rho. However, previous studies (17) have shown that LIM-kinase activation and cofilin phosphorylation occur in response to Rac, another member of the Rho family GTPases, but not to Rho. We therefore determined whether activation of Rho results in cofilin phosphorylation by LIM-kinase in vivo by expressing constitutively active V¹⁴-Rho and tagged cofilin in COS-7 cells (Fig. 3A). This experiment was done under conditions in which the activity of endogenous Rac was inhibited by expression of the dominant negative mutant N¹⁷-Rac, and that of endogenous Rho was inhibited by culture in serum-free medium (13). Expression of N¹⁷-Rac almost completely abolished the cofilin phosphorylation observed in cells expressing tagged cofilin alone, suggesting that endogenous Rac was activated under basal conditions and induced cofilin phosphorylation. In the presence of N¹⁷-Rac, V¹⁴-Rho increased cofilin phosphorylation in transfected cells, and this increase was inhibited by coexpression of a dominant negative ROCK mutant, ROCK-KDIA (14). These observations suggest that the Rho-ROCK pathway is linked to cofilin phosphorylation in vivo, and that the previous studies (17) may have masked this pathway by activation of endogenous Rac and Rho. We attempted to confirm this conclusion by expressing the DA mutant of LIMK2. However, this mutant functioned in a dominant negative manner in neither the Rho-mediated pathway nor the Rac-mediated pathway in our system (18). Finally, we investigated the link between Rho-ROCK signaling and the LIM-kinase-cofilin pathway at the morphological level. Overexpression of LIMK1 in HeLa cells induced the formation of thick, bundled stress fibers (Fig. 3B) that resembled those induced by active Rho or ROCK (14). Incubation of the transfected cells with Y-27632 resulted in the dissolution of these fibers, indicating that LIM-kinase collaborated with the Rho-ROCK pathway to induce stress fiber formation.

Our results indicate that LIM-kinase is phosphorylated and activated by ROCK downstream of Rho, and that LIM-kinase, in turn, phosphorylates cofilin. Because cofilin is essential for turnover of actin filaments (11, 19), our results suggest that Rho-ROCK signaling may stabilize actin filaments by inducing the phosphorylation and consequent inactivation of cofilin. Together with the results of other analyses (2, 20), our data provide insight into the pathways that link Rho to the actin cytoskeleton (Fig. 3C). Active Rho signals to two effectors, ROCK and mDia (a mammalian diaphanous homolog) (20). ROCK inactivates myosin phosphatase and cofilin, resulting in inhibition of actin depolymerization to stabilize formed F-actin and enhance-

ment of actomyosin contractility. mDia recruits profilin (20), likely promoting actin polymerization (21). These pathways thus may underlie neurite retraction as well as other Rho-mediated processes such as stress fiber formation (2). Rac, another member of the Rho family of GTPases, induces membrane ruffles and also activates LIM-kinase and triggers the phosphorylation of cofilin (17), but reduces actomyosin-based contractility (22). These observations suggest that Rho and Rac combine the same mechanism— inactivation of cofilin— differently with other mechanisms to produce different phenotypes. The observation that only a limited amount of cofilin is phosphorylated in response to cell stimulation (Fig. 1B) suggests that this mechanism may not influence the behavior of actin filaments throughout the cell; however, it certainly contributes to the temporal and spatial reorganization of specific actin cytoskeletons by the Rho family GTPases.

References and Notes

1. M. D. Welch, A. Mallavarapu, J. Rosenblatt, T. J. Mitchison, *Curr. Opin. Cell Biol.* **9**, 54 (1997).
2. S. Narumiya, *J. Biochem. (Tokyo)* **120**, 215 (1996); A. Hall, *Science* **279**, 509 (1998).
3. K. Kimura *et al.*, *Science* **273**, 245 (1996).
4. K. Burridge, M. Chrzanoska-Wodnicka, C. Zhong, *Trends Cell Biol.* **7**, 342 (1997).
5. M. Uehata *et al.*, *Nature* **389**, 990 (1997).
6. K. Kimura *et al.*, *J. Biol. Chem.* **273**, 5542 (1998); T. Matsui *et al.*, *J. Cell Biol.* **140**, 647 (1998).
7. K. Jalink *et al.*, *J. Cell. Biol.* **126**, 801 (1994).
8. M. Hirose *et al.*, *ibid.* **141**, 1625 (1998).
9. After LPA stimulation, N1E-115 cells were lysed with 10 mM tris-HCl (pH 7.5) containing 1 mM EGTA, 5 mM MgCl₂, 1 mM dithiothreitol, 1% (v/v) Triton X-100, and mixtures of phosphatase inhibitors and protease inhibitors. Lysates were centrifuged, and the supernatant, corresponding to 2 × 10⁴ cells, was subjected to two-dimensional electrophoresis with a linear pH gradient from 3.5 to 10, followed by autoradiography.
10. Purification and identification details of P1 and P2 proteins are available at www.sciencemag.org/feature/data/1041678.shl.
11. A. Moon and D. G. Drubin, *Mol. Biol. Cell* **6**, 1423 (1995).
12. S. Ono, N. Monami, H. Abe, T. Obinata, *J. Biol. Chem.* **269**, 15280 (1994).
13. In the transfection experiments in this study, COS-7 cells were transfected with combinations of the following vectors: pFL-C1-FLAG-tagged wild-type (WT) or S3A cofilin, pCAG-Myc-tagged ROCKΔ1 (14), pUCD2-SRα-FLAG-tagged LIMK1 (17), pUC-SRα-Myc-tagged LIMK 2 [I. Okano *et al.*, *J. Biol. Chem.* **270**, 31321 (1995)], pCMV5-FLAG-tagged N17-Rac (8), pEXV-Myc-tagged V14-Rho (14), and pCAG-Myc-tagged ROCK-KDIA (14). After transfection, cells were cultured for 15 hours in Dulbecco's minimum essential medium containing 10% fetal bovine serum (Fig. 1C) or in serum-free OPTI-MEM (Gibco) (Figs. 2B and 3A). In the experiments in Figs. 1C and 3A, the cells were then labeled for 4 hours with [³²P]orthophosphate (50 μCi/ml). Cells were lysed in 20 mM tris-HCl (pH 7.5) containing 1 mM EDTA, 1 mM EGTA, 5 mM MgCl₂, 5 mM 2-mercaptoethanol, 0.05% Triton X-100, and mixtures of phosphatase inhibitors and protease inhibitors. FLAG-tagged cofilin was immunoprecipitated with anti-FLAG (M2) affinity beads (Sigma) and subjected to SDS-polyacrylamide gel electrophoresis (SDS-PAGE) followed by autoradiography or immunoblot analysis (Figs. 1C and 3A). FLAG-tagged LIMK1 was immunoprecipitated and subjected to kinase assay (16) (Fig. 2B).
14. T. Ishizaki *et al.*, *FEBS Lett.* **404**, 118 (1997).

15. T. E. Morgan *et al.*, *J. Cell Biol.* **122**, 623 (1993); B. J. Agnew, L. S. Minamide, J. R. Bamberg, *J. Biol. Chem.* **270**, 17582 (1995); K. Moriyama *et al.*, *Genes Cell* **1**, 73 (1996).
16. His₆-tagged cofilin was expressed in *Escherichia coli* and His₆-tagged ROCKΔ4 (residues 1 to 477) was produced in Sf9 cells. Kinase reactions were done in a total volume of 23 μl at 30°C for 10 min with 50 μM [³²P]ATP (adenosine 5'-triphosphate) and 4 μg of either cofilin or histone type 2 as substrates in kinase buffer [25 mM Hepes-NaOH (pH 7.5), 10 mM MgCl₂, 5 mM MnCl₂, 0.1 mM EGTA, 0.05% Brij 35, 5 mM 2-mercaptoethanol, phosphatase inhibitors, and protease inhibitors].
17. S. Arber *et al.*, *Nature* **393**, 805 (1998); N. Yang *et al.*, *ibid.*, p. 809.

18. M. Maekawa *et al.*, unpublished data.
19. P. Lappalainen and D. G. Drubin, *Nature* **388**, 78 (1997); M.-F. Carlier *et al.*, *J. Cell Biol.* **136**, 1307 (1997).
20. N. Watanabe *et al.*, *EMBO J.* **16**, 1307 (1997).
21. D. Pantaloni and M.-F. Carlier, *Cell* **75**, 1007 (1993).
22. L. C. Sanders, F. Matsumura, G. M. Bokoch, P. de Lanerolle, *Science* **283**, 2083 (1999).
23. Supported by grants from the Ministry of Education, Science and Culture of Japan and from the Human Frontier Science Program. We thank E. Nishida, I. Yahara, and T. Doi for advice, and A. Shinohara for mass spectrometry. M.M. thanks S. Maekawa for encouragement.

11 May 1999; accepted 1 July 1999

Fas Ligand: A Sensor for DNA Damage Critical in Skin Cancer Etiology

Laurie L. Hill, Allal Ouhtit, Susan M. Loughlin, Margaret L. Kripke, Honnavara N. Ananthaswamy, Laurie B. Owen-Schaub*

DNA-damaged cells can either repair the DNA or be eliminated through a homeostatic control mechanism termed "cellular proofreading." Elimination of DNA-damaged cells after ultraviolet radiation (UVR) through sunburn cell (apoptotic keratinocyte) formation is thought to be pivotal for the removal of precancerous skin cells. Sunburn cell formation was found to be dependent on Fas ligand (FasL), a pro-apoptotic protein induced by DNA damage. Chronic exposure to UVR caused 14 of 20 (70 percent) FasL-deficient mice and 1 of 20 (5 percent) wild-type mice to accumulate p53 mutations in the epidermis. Thus, FasL-mediated apoptosis is important for skin homeostasis, suggesting that the dysregulation of Fas-FasL interactions may be central to the development of skin cancer.

In the United States, nearly 1,000,000 persons will develop nonmelanoma skin cancer (NMSC) (basal and squamous cell carcinoma) this year. Although death from NMSC is rare, these patients experience a substantially increased mortality from other cancers (20 to 30% higher), suggesting that skin cancer susceptibility may be linked to the development of noncutaneous malignancies (1). UVR in sunlight is the principal carcinogen, serving as initiator and promoter for most skin tumors (2). UVR elicits p53-dependent apoptosis in DNA-damaged keratinocytes (sunburn cells), presumably as a "guardian of the tissue" response to eradicate precancerous cells in the skin (3). This p53-driven response, termed "cellular proofreading" (3), erases rather than repairs DNA damage. Mice deficient in p53 (p53-null) have reduced sunburn cell formation and increased susceptibility to UVR-induced skin carcinogenesis (2, 4), implicating apoptosis as a critical event in skin carcinogenesis. Fas and FasL are complementa-

ry receptor-ligand proteins eliciting apoptosis (5). Although Fas and FasL are induced by nuclear factor kappa B activation (6–8), wild-type p53 is essential for the transcriptional up-regulation of Fas after DNA damage (9–11). Thus, Fas and FasL may serve as external pro-apoptotic sensors of DNA damage-mediated cellular proofreading.

To investigate Fas and FasL expression in normal skin after UVR, we shaved C3H/HeJ wild-type mice, exposed them to a single dose of ultraviolet (UV) light (5 kJ/m²) (12), and harvested epidermal skin sections for immunohistochemistry (13). Nonirradiated skin had little Fas and FasL expression (Fig. 1). Both Fas and FasL expression were potentially induced in the epidermis by UVR as early as 3 and 6 hours after irradiation, with maximal induction of both proteins occurring at 12 hours. By 24 hours, UVR-induced Fas and FasL expression in the epidermis was similar to that observed before treatment. Dermal Fas expression (hair follicles and sebaceous glands), in contrast, remained elevated at this time point. These results indicate that both Fas and FasL are transiently up-regulated only in the normal epidermis by UVR exposure, as previously reported in human skin (8).

Because the proapoptotic proteins Fas and

Department of Immunology, University of Texas, M. D. Anderson Cancer Center, Houston, TX 77030, USA.

*To whom correspondence should be addressed. E-mail: lowensch@mdanderson.org